Available online at www.sciencedirect.com

ScienceDirect

Energy Procedia 101 (2016) 1280 – 1287

Energy Procedia

71st Conference of the Italian Thermal Machines Engineering Association, ATI2016, 14-16 September 2016, Turin, Italy

Hybrid CFD-source terms modelling of a diffuser-augmented vertical axis wind turbine

Stefano Letizia*, Stefania Zanforlin

Department of Energy, Systems, Territory and Constructions Engineering, University of Pisa, l.go L. Lazzarino, 56122 Pisa, Italy

Abstract

In order to reduce the calculation time in the analysis of a diffuser augmented H-Darrieus wind turbine (DAWT), a hybrid CFD-source terms 2D approach, relying on a new experimental-based dynamic stall model, was adopted. This method consists in solving the blades load by means of an analytic model, whereas the overall flow field is calculated through a simplified CFD. The new model was compared with a complete CFD exhibiting a satisfying agreement both for the case of a bare turbine and an unoptimized DAWT. By virtue of the rapidity of the new model, an optimization analysis of the diffuser design was carried out. A great power gain was achieved, thanks to unexpected aerodynamic phenomena, but an even greater increase of the frontal area was necessary. The critical issues of the modelling approach and the proposed DAWT are discussed.

Peer-review under responsibility of the Scientific Committee of ATI 2016.

Keywords: wind turbine; source term model; dynamic stall; diffuser; augmentation.

1. Introduction

The Vertical Axis Wind Turbine technology (VAWT), in particular the lift-driven concept, is gaining a renewed interest among the researcher by virtue of the ability to maintain an acceptable efficiency in highly turbulent, unstructured flows [1-6]. Simulating the operation of these machines is a challenging issue, because of the unsteady

* Corresponding author. Tel.: 3421557566.
E-mail address: sxl162231@utdallas.edu

Peer-review under responsibility of the Scientific Committee of ATI 2016.
doi:10.1016/j.egypro.2016.11.144

aerodynamic regime in which the blades operate [7, 8] that triggers the dynamic stall [9, 10] and greatly affects the lift and drag characteristics of the airfoils [11]. A straightforward way to model a Darrieus rotor is the BEM approach [12] that consists in adopting a simplified aerodynamic analysis of the flow near the blade and solving the momentum balance across the single [13], multiple [14-18] or double-multiple [19, 20] streamtubes passing through the rotor. These models give a fast response but they disregard important phenomena [12], such as turbulent mixing and 2D effects. Recently, CFD have become a reliable alternative to classic models for simulating VAWTs [21]. However, a very high computational effort is required to obtain a converged flow field [8], mainly due to the solution of the flow near the blades, where phenomena characterized by short length and time-scales occur. Recently, inspired by the well-known actuator disk approach adopted for HAWTs, some authors [22-25] have developed hybrid CFD-BEM models for VAWTs combining the accuracy of CFD and the rapidity of BEM models. According to this approach, the load on the blades is estimated by means of a semi-empirical formulation, whereas the overall flow field is solved by CFD, once appropriate momentum source terms are introduced.

In the first part of this work, a new hybrid CFD-BEM approach relying on a new, experiment-based dynamic stall model, is presented. The results were compared to that of a full-CFD of a bare turbine, exhibiting good agreement.

In a second time, a diffuser was introduced in order to enhance the power production. The diffuser, namely a channeling device increasing the flow rate through the rotor [26], whose benefic effects on Cp were recently confirmed by thorough experiments ([27] for a HAWT, [28] for a VAWT), is a controversial technology. In fact, when the Cp is based on the exit area, the benefits are not clear [29], yet some authors claim that Betz limit can be exceeded even considering this form of the coefficient of power [29, 30]. In this study, after the verification of the agreement between CFD and the new model for an unoptimized DAWT, thanks to the short response time achievable by means of the hybrid approach, the optimization of the diffuser was performed and the results justified.

2. CFD validation

To verify the present CFD accuracy, the experiment and the simulations by Balduzzi et al. [8] were reproduced. The mesh characteristics and the solver setup were taken from the reference article [8]. A mesh made up of 530000 elements with sliding interfaces was built. The fluid was compressible, as in the reference study. However, the additional computational effort and the improvement in the flow field associated with compressibility modelling resulted both negligible, as the authors of the reference study state themselves. The timestep corresponded to 0.35° of rotation. The result is depicted in Fig. 1. The differences between the present and the reference study are mainly due to a shallower convergence of the average torque here adopted to limit the huge computational effort (0.5% of relative variations between two consequent revolutions instead of 0.1%). The present convergence criterion is still more conservative than the usual 1% limit usually adopted in literature [8]. The comparison between the Cp-TSR curves obtained with different thresholds on the torque confirms the remarkable influence of such a parameter. However, the overall trend is satisfactory.

After the validation, a sensitivity analysis was carried out to find a time-effective set of simulation parameters. With a mesh made up of 260000 cells and a timestep corresponding to 0.66° of rotation, negligible changes in the Ct curves were observed. Therefore, this new setup was adopted in the continuation of the work, except for the simplified domains required by the hybrid model, where incompressible fluid and less accurate discretization were sufficient, since the flow field around the blades is not modeled.

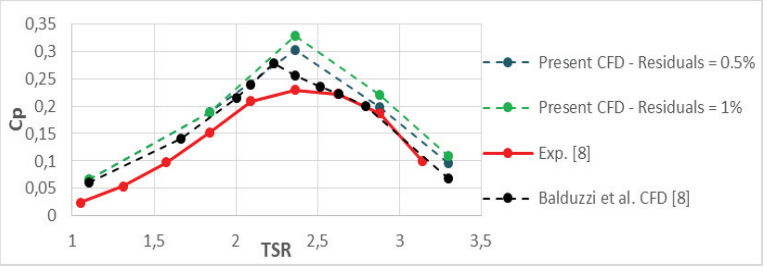

Fig. 1. Comparison between present CFD, reference CFD and experiment.

3. Actuator ring model (AR)

The Actuator Ring model can be considered as the 2D version for the Actuator Cylinder approach [31]. The rotor is replaced, in the simplified CFD domain, by a ring discretized in several elements, where source terms, representing the forces exerted by the blades on the flow averaged over a revolution, are imposed. For each ring element, the CFD provides the absolute local flow velocity ($\boldsymbol{U}$). The relative velocity ($\boldsymbol{W}$), that, according to classic BEM theory, is the vector sum of the local velocity ($\boldsymbol{U}$) and the rotational velocity ($\boldsymbol{\omega R}$) of the blade [12], is then known. Once the angle of attack is derived by means of trigonometric considerations, the dynamic stall model (Chap. 3.1) provides the drag ($\boldsymbol{D}$) and lift ($\boldsymbol{L}$) forces. These forces, projected along the x-y axis, changed in sign, are the loads experienced by the fluid. The related momentum source terms $\boldsymbol{S_{i,j}}$ were evaluated in analogy with [22] as:

$$S_{i,j} = F_{i,j} \frac{N\Delta\theta_j}{2\pi} \frac{1}{A_j} \text{ [N/m}^2\text{]} \quad (1)$$

Where $F_{i,j}$ is the force along the i-th direction in the j-th of the N sectors of angular extension $\Delta\theta_j$ and surface A_j in which the rotor swept area is discretized.

3.1 Dynamic stall model

The present model derives from the Larsen et al. model [32], but appropriate modifications were made (new tuning, drag, different static lift and flow detachment modeling), thanks to the possibility to access a NASA study on oscillating airfoils [33] providing a wide selection of experimental data. The lift and drag characteristics are mainly affected by the delay in the constitution of the circulation when the boundary layer is attached, added mass forces, dynamic of the detachment/reattachment of the boundary layer and leading edge vortex (LEV), a vortex that sheds from the airfoil surface causing a sudden lift and drag decay. In the present model, the lift is evaluated as follows:

$$Cl_{tot} = (Cl_0 + Cl_{nc})\, f + Cl_{min}(1 - f) + Cl_v \quad (2)$$

Where:

- Cl_0 is the ideal lift accounting for the delay in the constitution of the circulation under attached flow conditions via a Green-type formula
- Cl_{nc} corresponds to the added mass contribution, as stated by Theodorsen [34]
- f is a coefficient ranging from 1 (attached flow) to 0 (completely detached boundary layer) and its dynamics is simulated by means of a first order differential equation
- Cl_{min} is the lift under fully stalled conditions, taken from static data [35] as a linear function of angle of attack and Reynolds number
- Cl_v is the contribution form the LEV that makes the lift exceed the linear lift when it is placed on the blade and causes a rapid plunge of the lift when it is convected far away; it is modeled through a first order differential equation; the angle of attack corresponding to the LEV shedding was approximated from a linear fit of ten experimental curves [33] as a function of Reynolds and oscillation frequency

The drag modeling was not present in the original model but was derived from the lift formulation:

$$Cd_{tot} = Cd_{max}\,(1 - f) + Cd_{min}\, f + Cl_v \tan(\square) \quad (3)$$

Where Cd_{max} and Cd_{min} come once again from static data [35] and for the LEV contribution the straightforward flat plate approximation was adopted [36]. The model contains four unknown time constants that were tuned reproducing the lift hysteresis cycle of a NACA0012 airfoil in ref. [33] (the first frame of Fig. 2). The comparison between the present model results and the experimental data is provided in Fig. 2. The agreement was considered satisfactory for the present purposes. The accuracy of the model for other airfoil sections was not verified.

3.2 Solving strategies

The kinematic scheme and the dynamic stall model were implemented in a UDF in Fluent. Being the load on the blades and the flow field tightly coupled, the overall solution can be considered physically meaningful only when it exhibits a stationary or periodic regime. Therefore, for the present case, three different strategies, depending on the complexity of the studied configuration, were adopted:

- steady-iterative: the CFD simulations are steady and the loads are calculated iteratively at the end of each simulation until a convergence criterion on the torque is met;
- transient-iterative: the CFD simulation are transient and the loads are calculated once in a fixed period;
- pure transient: in this case the force are recomputed by AR every timestep of the transient simulations.

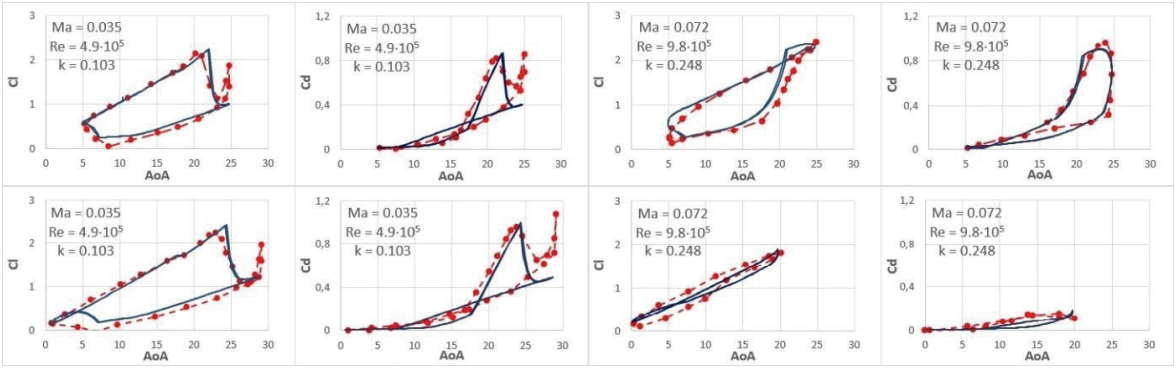

Fig. 2. Lift and drag coefficient for oscillating airfoils at different reduced frequency (k), Mach number (Ma) and Reynolds number (Re): comparison between dynamic stall model (blue) and experimental data (red) [33].

4. AR vs. CFD

A three-bladed H-Darrieus having a diameter of 2m was simulated by means of both CFD and AR to verify the agreement. The blades had a NACA0012 section with virtual camber that almost annuls the flow curvature effect [37] and permits the adoption of the proposed dynamic stall model without modifications.

4.1 Bare turbine

The steady-iterative method was sufficient for the bare turbine case. This made obviously unaffordable the vortex shedding simulation, but the calculation time passed from 40 hours to less than 30 minutes.

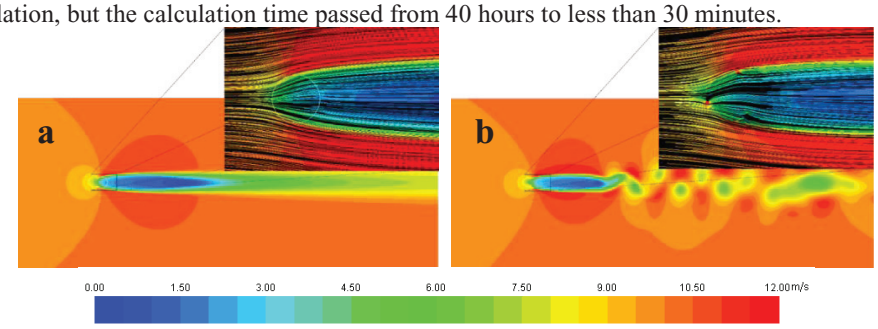

Fig. 3. Bare turbine, TSR 2.7, Velocity magnitude: (a) AR; (b) CFD.

The qualitative agreement between the two flow fields for the highest Cp TSR is satisfactory (remember that the AR only reproduces the velocity averaged over a revolution and, therefore, cannot consider the local perturbations induced by the blades). The number of elements passed from 250000 for CFD to 40000 for AR (that resulted even

redundant in the successive sensitivity analysis). The curves of coefficient of torque ($Ct = \frac{Torque}{\frac{1}{2}\rho U^2 RA}$) are reported in Fig. 4 for three different TSR, from stall conditions to fully attached flow. An acceptable qualitative and quantitative agreement can be observed. The first part of the downwind path shows poor agreement, probably due to an overestimation of added mass term. A different threshold TSR before the stall occurrence was detected, but its influence was negligible. At the end of this part, a wide sensitivity analysis on mesh, timestep in the dynamic stall model, ring thickness, number of sources terms was carried out, confirming the previous results.

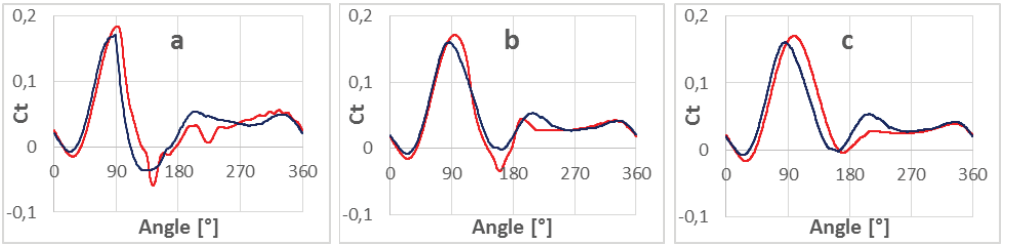

Fig. 4. Bare turbine Ct curves of a single blade from CFD (red) and AR (blue) for different TSR: (a) 2.3; (b) 2.5; (c) 2.7.

4.2 *Turbine with diffuser*

A diffuser formed by two Selig 1223 wings having a null angle of attack was created. A sensitivity analysis indicated a 360000 elements cells as the more suitable for CFD, whereas for the AR a 30000 cells mesh and a timestep of 0.02s were sufficient to catch the unsteady wake development. The method was transient-iterative.

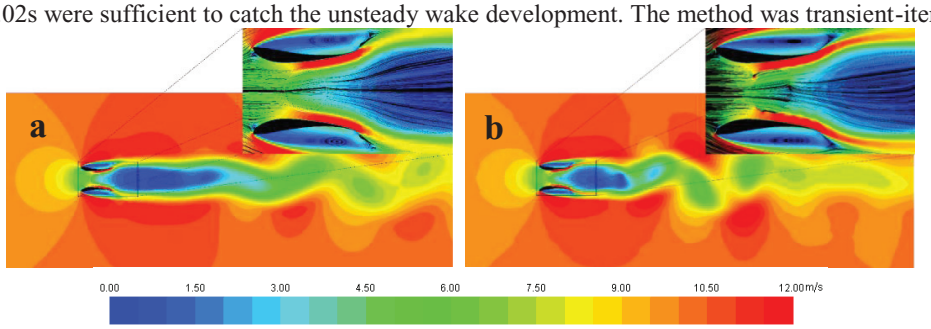

Fig. 5. Diffuser-augmented turbine, TSR 2.7, Velocity magnitude: (a) AR; (b) CFD.

In this case, also the vortex shedding in the far wake is reproduced by the AR, but the fluctuations do not affect the solution in the rotor zone.

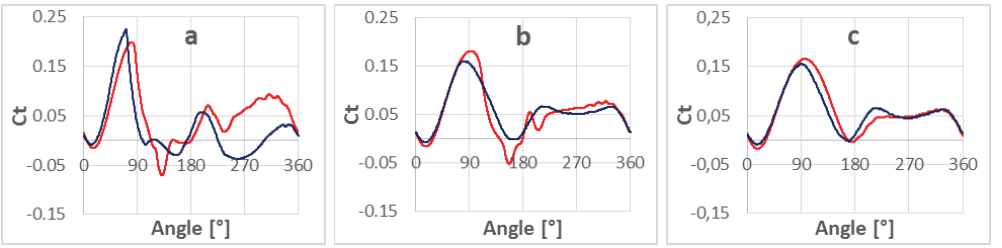

Fig. 6. Diffuser-augmented turbine, Ct curves of a single blade from CFD (red) and AR (blue) for different TSR: (a) 2.3; (b) 2.5; (c) 2.7.

AR fails to predict the Ct for the lower TSR case (2.3) where the stall of the blade is deep and the modeling through the semi-empiric dynamic stall model becomes very challenging. Fortunately, this point is quite far from the

operative condition. Instead, AR was able to reproduce the main effects of the diffuser, such as the upwind peak fattening and the downwind Ct upshift [38], as the comparison of Fig. 4 and Fig. 6 shows.

4.3 Cp vs. TSR

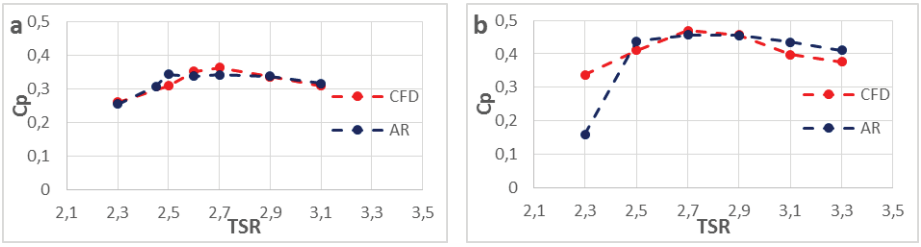

Fig. 7. Ct vs. TSR curves for AR (blue) and CFD (red): (a) Bare turbine; (b) Diffuser-augmented turbine.

The Cp values are in good agreement, except for the TSR associated with the occurrence of a deep stall, as already stated. However, the maximum Cp, the overall trend and the diffuser effect are well reproduced by AR.

5. Optimization

The fast AR model permitted to carry out, in a reasonable time, a One-Factor-At-Time (OFAT) analysis of the main geometrical parameters expected to affect the overall performance of the DAWT. Since the chord of the wing forming the diffuser was kept constants to 2.5D assuming a size constraint, the optimization focused on the divergence angle (α), the throat area (H) and the turbine position (W).
The OFAT analysis can be summarized in three phases:

- α = variable, H = 1.3 D, W = 0: in this phase the higher angle before the stall occurrence inside the diffuser was surprisingly 40 degrees; such a behavior, stressed by other authors [27, 39], and confirmed by complete CFD simulations (Fig. 8), can be related to a fluid pre-rotation induced by the turbine trust and to the smoothing of the adverse pressure gradient occurring by virtue of the pressure field induced by the turbine;
- α = optimized, H = variable, W = 0: the reduction of the throat area had positive influences both on the power output and on the boundary layer attachment inside the diffuser; this permitted to increase the divergence angle up to 50 degrees
- α = optimized, H = optimized, W = variable: the results by Malipeddi et al. [40] were confirmed and the optimal position in terms of power output was find out to be exactly the throat

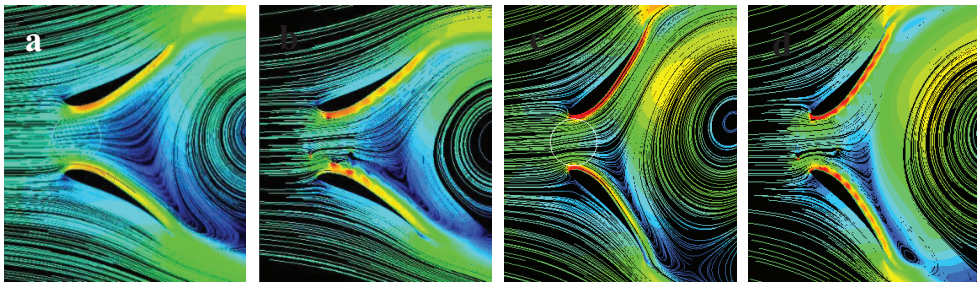

Fig. 2. α = 30°, H = 1.3D, W = 0, U = 10 m/s, TSR 3.5: (a) AR, (b) CFD; α = 50°; H = 1.15D, W = 0, U = 5 m/s, TSR 4.3: (c) AR, (d) CFD.

In the end, the optimal configuration had a divergence angle of 50 degrees, a throat area of 1.15 D and the turbine placed in throat. When tested in a very large domain (300D x 600D), therefore unaffected by blockage concerns, the maximum Cp reached 1.32, 3.8 times the bare turbine value. However, the frontal area became 5 times higher, indicating that the present diffuser does not allow for an improved wind power exploitation, being equal the frontal

area. Fig 9. shows the effects of the diffuser on the turbine in terms of performance enhancement and shedding-induced fluctuations. Unfortunately, the Cp slightly decreases compared to that of the bare turbine when it is based on the overall frontal area (i.e. the diffuser exit section). Concerning the model, as already mentioned, the results were confirmed by full CFD in two cases: for the 30 degrees diffuser (Fig. 8 a, b) there was a good agreement; for the optimal configuration (Fig. 8 c, d), the CFD solutions showed an unstructured pattern even after 500 revolutions, but the boundary layer attachment and the Cp augmentation were confirmed. Probably, in the accurate CFD, the flow field needed a longer and unaffordable time to reach the periodic regime. This discrepancy between the two approaches in the very critical regime that the boundary layer undergoes when such a great divergence is adopted, has been interpreted as an unavoidable shortcoming due to the time-averaged modelling of the aerodynamic loads, that in some way smooths the fluctuations induced by the blade alternate passage. An improvement of the model would be the adoption of an actuator line or surface approach [41, 42]. Notwithstanding these minor flaws, however, the calculation time with AR was almost 100 time shorter than that of CFD.

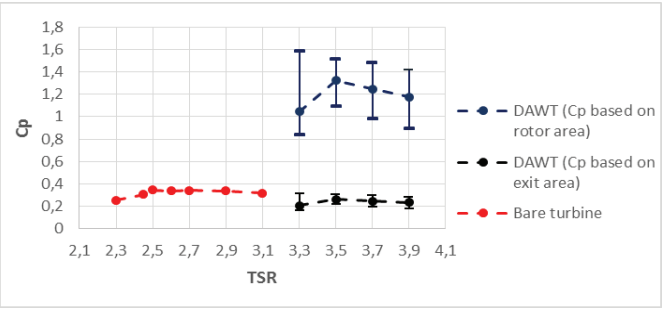

Fig 9. Cp vs. TRS curves for DAWT and bare turbine from AR.

6. Conclusions

A new hybrid CFD-source terms model for the aerodynamics of an H-Darrieus turbine was implemented. The model calculates the aerodynamic load on the blades by means of an analytical semi-empiric method. An improved indicial model to simulate the effects of the dynamic stall on lift and drag was adopted. For the solution of the overall momentum and mass balances, a CFD solver operating in a simplified domain was employed. The new model was able to reproduce the torque evolution of a bare turbine for different TSR in close agreement with complete CFD. The boundary layer separation occurs at a TSR slightly lower for AR (2.45) than for CFD (2.5), but this was expected, since this threshold TSR represents a very challenging condition to reproduce. When the diffuser was introduced, the AR failed to capture the unstructured pattern of the torque curve under deep stall condition, but was capable of predicting the effects of the new device in the turbine. The AR model was successfully adopted in an OFAT optimization of the diffuser geometry where unexpected phenomena, such as an impressive boundary layer attachment and a vigorous vortex shedding, were detected and confirmed by CFD. The new diffuser-augmented turbine had a peak Cp of 1.32 (almost 4 times higher than the original Cp) that however falls to 0.26 when the same coefficient is based on the frontal area. This lower conversion efficiency coupled to the increased construction and operation complexity, could nullify the cost-effectiveness of the diffuser against conventional systems. The proposed device could become attractive in environments in which a vertical extension limit holds, since a very short and efficient DAWT could be feasible. The most interesting result arising from the present study was the very time-sparing modelling that the hybrid model permitted. The calculation time was reduced by a factor of 100 with an acceptable loss of accuracy. The proposed model could be successfully employed, especially in an upgraded 3D version, to study the interactions between the machine and the environment or the wake effects in turbine farms.

Acknowledgements

This study has been financially supported by University of Pisa: Progetti di Ricerca di Ateneo (PRA) 2015 “Metodi e tecniche innovative per l'integrazione di sistemi per l'energia elettrica e termica”.

References

[1] Eriksson S, Bernhoff H, Leijon M. Evaluation of different turbine concepts for wind power. Ren. & Sust. En. Rev. 2008; 12:1419–34.
[2] Toja-Silva F, Colmenar-Santos A, Castro-Gil A. Urban wind energy exploitation systems: Behavior under multi directional flow conditions, Opportunities and challenges, Ren. & Sust. Energy Rev. 2013; 24:364-368.
[3] Riegler H. HAWT versus VAWT: small VAWTs find a clear niche. Refocus 2003;4(4):44 – 6.
[4] Sharpe T, Proven G, Crossflex: Concept and early development of a true building integrated WT, Energy Build. 2010; 42 12: 2365-75.
[5] Mertens S, van Kuik G, van Bussel G. Performance of an H-Darrieus in the skewed flow on a roof, JSSE 2003; 125:433–40.
[6] Jamieson P, Innovation in Wind Turbine Design, First Edition; 2011.
[7] Paraschivoiu I, Wind Turbine Design with Emphasis on Darrieus Concept, Polytechnic International Press, Canada; 2002.
[8] Balduzzi F, Bianchini A, Maleci R, Ferrara G, Ferrari L, Critical issues in the CFD simulation of Darrieus wind turbines, Ren. Energy 2016; 85:419-435.
[9] Buchnera AJ, Lohrya MW, Martinellia L, Soriab J, Smitsa AJ, Dynamic stall in vertical axis wind turbines: Comparing experiments and computations, Journal of Wind Engineering and Industrial Aerodynamics 2015; 146:163–171.
[10] Almohammadia KM, Inghamb DB, Mab L, Pourkashanian M. Modeling dynamic stall of a straight blade VAWT, Journal of Fluids and Structures 2015; 57:144–158.
[11] McCroskey WJ. The Phenomenon of Dynamic Stall, NASA Technical Memorandum 81264; 1981.
[12] Islam M, David SKT, Fartaj A. Aerodynamic models for Darrieus-type straight-bladed vertical axis wind turbines. Ren. & Sust. Energy Rev. 2008; 12:1087–1109.
[13] Templin RJ, Aerodynamic performance theory for the NRC vertical-axis wind turbine. NRC Lab.report LTR-LA-190; 1974.
[14] Wilson RE, Lissaman PBS. Applied aerodynamics of wind power machines. Oregon St. Univ.; 1974.
[15] Strickland JH. A performance prediction model for the Darrieus turbine. In: Int. symp. on wind energy systems, Cambridge, UK;1976.
[16] Muraca RJ, Stephens MV, Dagenhart JR. Theoretical performance of cross-wind axis turbines with results for a catenary vertical axis configuration. USA: NASA TMX-72662;1975.
[17] Sharpe DJ. A theoretical and experimental study of the Darrieus vertical axis wind turbine. School of Mechanical, Aeronautical & Production Engineering. Kingston Polytechnic. Research report. October, 1977.
[18] Read S, Sharpe DJ. A next ended multiple streamtube theory for VAWTs. Cranfield, UK: 2nd BWEA workshop 1980; p. 65-72.
[19] Paraschivoiu I. Double-multiple streamtube model for darrieus wind turbines. 2nd DOE/NASA wind turbines dynamics workshop, NASA CP-2186, Cleveland, OH, February, 1981. p. 19–25.
[20] Paraschivoiu I, Delclaux F. Double multiple streamtube model with recent improvements. J Energy 1983; 7:250
[21] Raciti Castelli M, Englaro A, Benini E, The Darrieus wind turbine: Proposal for a new performance prediction model based on CFD, Energy 2011; 36(8):4919-4934
[22] Torresi M, Fortunbato B, Camporeale S. Modello CFD per il calcolo delle prestazioni e degli effetti di scia di, La Termotecnica, 2013.
[23] Antheaume S, Maitre T, Achard JL. Hydraulic Darrieus turbines efficiency for free fluid flow conditions versus power farms conditions, Ren. Energy 2008; 33(10):2186-2198
[24] Dominguez F, Achard JL, Zanette J, Corre C. Fast power output prediction for a single row of ducted cross-flow water turbines using a BEM-RANS approach, Ren. Energy 2016; 89:658-670.
[25] Georgescu AM, Georgescu SC, Perte AM, Badea I. Time efficient computing of the power coefficient for a ducted Achard turbine, U.P.B. Sci. Bull., Series D, Vol. 74, Iss. 4, 2012.
[26] Bontempo R, Manna A. Performance analysis of open and ducted wind turbines. Applied Energy 2014; 136:405–416.
[27] Ohya Y, Karasudani T, Sakuri A, Abe K, Inoue M. Development of a shrouded wind turbine with a flanged diffuser. J Wind Energy and Ind Aerodynaics 2008; 96:524-539.
[28] Ponta F, Dutt GS, An improved vertical-axis water-current turbine incorporating a channelling device, Ren. Energy 2000; 20:223-241.
[29] Van Bussel, GJW. The science of making more torque from wind: Diffuser experiments and theory revisited. J. Phys. Conf. Ser. 2007; 75:1–12.
[30] Hjort H, Sorsen H, A Multi-Element Diffuser Augmented Wind Turbine, Energies 2014; 7:3256-3281.
[31] Madsen HA. The actuator cylinder flow model for vertical axis wind turbines. PhD dissertation, Aalborg University Centre, 1982.
[32] Larsen JW, Nielsena SRK, Krenk S. Dynamic stall model for wind turbine airfoils, Journal of Fluids and Structures 2007; 23:959–982
[33] McAlister KW, Pucci SL, McCroskey WJ, Carr LW. An Experimental Study of Dynamic Stall on Advanced Airfoil Sections, NASA Technical Memorandum 84245, 1982.
[34] Theodorsen T. General Theory of Aerodynamic Instability and the Mechanism of Flutter. Technical Report 496, NACA, 1935.
[35] Sheldahl ER, Klimas PC. Aerodynamic Characteristics of Seven Symmetrical Airfoil Sections Through 180-Degree Angle of Attack for Use in Aerodynamic Analysis of Vertical Axis Wind Turbines. SANDS0-2114.
[36] Ortiz X, Rival D, Wood D. Forces and Moments on Flat Plates of Small Aspect Ratio with Application to PV Wind Loads and Small Wind Turbine Blades, Energies 2015; 8(4):2438-2453
[37] Balduzzi F, Bianchini A, Ferrara G, Ferrari L, Maleci R. Blade design criteria to compensate the flow curvature effects in H-Darrieus wind turbines, J. Turbomach. 2015; 137(1):1-10.
[38] Zanforlin S, Letizia S. Improving the performance of wind turbines in urban environment by integrating the action of a diffuser with the aerodynamics of the rooftops, Energy Procedia 2015; 82:774–781
[39] Maître T, Mentxaka Roa A, Pellone C, Achard JL. Numerical 2D hydrodynamic optimization of channeling devices for cross-flow water turbines, U.P.B. Sci. Bull., Series D, Vol. 72, Iss. 1 2010.
[40] Malipeddi AR, Chatterjee D. Influence of duct geometry on the performance of Darrieus hydroturbine, Ren Energy 2012; 23:292-300.
[41] Bachant P, Goude A, Wosnik M. Actuator line modeling of vertical-axis turbines, Wind Energ. 2016; 00:1–23.
[42] Shen WZ, Zhang JH, Sørensen JN. The actuator surface model: A new Navier–Stokes based model for rotor computations, Journal of Solar Energy Engineering, Vol. 131, No. 1, 2009, p. 011002